This study explores a multi-reflection time-of-flight mass spectrometer (TOFMS) based on transaxial electrostatic mirrors providing spatial and energy time-of-flight focusing of the ion beam. Analysis of existing solutions reveals that spatial-energy time-of-flight focusing in compact TOFMSs is achieved using additional focusing elements, which complicates the design, limits resolution, and reduces sensitivity.

This paper demonstrates that three-electrode transaxial mirrors enable simultaneous spatial and energy time-of-flight focusing of ions without the use of additional focusing elements. Monte Carlo simulation of the beam dynamics has made it possible to determine the trajectories and flight times of ions under various initial conditions.

It was found that two closely spaced vertical focusing modes provide time-of-flight focusing of ions with a relative energy spread of $\varepsilon = \pm 0.001$. ***A mass resolution of 10,000 at half-maximum confirms the high efficiency of the proposed structure. The spatial distributions of the ion beam demonstrate stable focusing in the detector plane when modeling particles larger than 1000.***

The results are attributed to the features of transaxial geometry, which enables three-dimensional spatial and energy time-of-flight focusing. The practical significance of this work is the applicability of such multi-reflector mass analyzers in laboratory and space research where a combination of high resolution and instrument compactness is required

Keywords: multi-reflector time-of-flight mass spectrometers, transaxial electrostatic mirror, analytical expressions for potential

UDC 537.86:681.518:004.942
DOI: 10.15587/1729-4061.2025.346298

OPTIMIZATION OF A MULTI-REFLECTION TIME-OF-FLIGHT MASS SPECTROMETER WITH TRANSAXIAL MIRRORS PROVIDING SPATIAL AND ENERGY TOF FOCUSING

Tilektes Shugayeva
Corresponding author
PhD, Senior Lecturer*
E-mail: tlektes.tleubaeva@gmail.com
Igor Spivak-Lavrov
Doctor of Physical and Mathematical Sciences, Professor*
Orda Baisanov
Candidate of Physical and Mathematical Sciences, Senior Lecturer
Department of Construction and Operation Radio-Electronic Equipment
T. Y. Begeldinov Military Institute of Air Defense
Alia Moldagulova ave., 38, Aktobe, Republic of Kazakhstan, 100026
Amangul Amantayeva
Doctoral Student*
*Department of Physics
K. Zhubanov Aktobe Regional University
A. Moldagulova str., 34, Aktobe, Republic of Kazakhstan, 030000

Received 29.09.2025
Received in revised form 28.11.2025
Accepted date 08.12.2025
Published date 23.12.2025

How to Cite: *Shugayeva, T., Spivak-Lavrov, I., Baisanov, O., Amantayeva, A. (2025). Optimization of a multi-reflection time-of-flight mass spectrometer with transaxial mirrors providing spatial and energy tof focusing. Eastern-European Journal of Enterprise Technologies, 6 (5 (138)), 34–42. https://doi.org/10.15587/1729-4061.2025.346298*

1. Introduction

The emergence and widespread use of new pulsed ion sources has stimulated intensive development in the field of gridless multipass time-of-flight mass spectrometers. These devices have already approached the resolution of static mass spectrometers, while offering a number of significant advantages: they are characterized by higher sensitivity, are virtually unlimited in mass range, and enable simultaneous recording of all masses during a single ion packet pass. Furthermore, state-of-the-art ion detection methods allow spectra to be obtained with short analysis times and high recording speeds.

Time-of-flight mass reflectrons are known, in which the ion beam is reflected from a region with a buoyant potential and then enters a detector. This configuration allows for spatial and energetic focusing of the ion beam [1–3]. The operating principle of mass reflectrons, their historical aspects, and the evolution of computational methods are discussed in detail and summarized in [1]. Further advancement and expansion of TOFMSs are discussed in [2], while modern structural solutions and approaches to designing high-resolution TOFMSs are reported in [3]. In a reflectron, ions with higher energies penetrate deeper into the region of the expulsion field, resulting in their path being longer compared to ions with lower energies. This makes it possible to fabricate mirrors in which ions of different energies pass into the detector simultaneously, thereby ensuring spatial and time-of-flight focusing.

State-of-the-art multi-reflectance time-of-flight mass spectrometers demonstrate significant potential for increasing the length of flight and achieving high resolution. However, their effectiveness depends significantly on the precision of electrostatic field generation and the system's ability to provide stable spatial-energy time-of-flight focusing with minimal aberrations. This has fueled interest in designing new types of electrostatic fields and mirror systems that allow for targeted control over potential distribution and op-

timized ion beam dynamics. Generating such fields enables the construction of compact and more accurate next-generation mass analyzers. This improves measurement quality and expands their application ranges from laboratory experiments to space exploration.

Thus, the development and research of time-of-flight mass reflectrons represents a relevant and promising area of modern physical electro-optics.

2. Literature review and problem statement

Recently, research into the design of multi-cascade or multi-reflection TOFMSs based on gridless planar mirrors has been actively advancing. Among known multi-reflection systems, it is the planar configuration formed by two parallel mirrors that provides open ion trajectories and, as a result, enables the detection of a full mass range. Studies on multi-reflection configurations with planar mirrors show that such systems can significantly increase the flight length and improve temporal focusing [4, 5]. However, most such systems require the use of additional focusing elements, which complicates the design and reduces the beam transmission efficiency.

Studies of gridless mirrors have proposed solutions that eliminate ion scattering on grids [6]. Despite the absence of grids, such mirrors require a highly accurate electrostatic field profile. The slightest deviations in the potential distribution lead to disruption of temporal focusing, making the implementation of such systems technically challenging and sensitive to electrode parameters.

A high-performance multi-reflector time-of-flight system designed for the analysis of short-lived isotopes is reported in [7]. The structure provides stable temporal focusing but it includes multi-stage reflector sections and complex matching elements, making it primarily applicable to large-scale experimental setups. Transferring such solutions to compact systems is difficult.

Improved multi-reflection schemes described in [8] demonstrate high resolution under strictly defined ion packet formation conditions. However, such systems remain sensitive to voltage stability and geometric parameters, limiting their use in simple and compact analyzers. Hybrid quadrupole multi-reflection schemes discussed in [9, 10] expand the range of detectable masses but require complex matching devices and high-precision voltage sources.

Studies on secondary ion mass spectrometry with a multi-reflection architecture [11] demonstrate high trajectory stability and high resolutions. However, the approach is focused on specific SIMS tasks and relies on experimental parameter tuning. The models obtained in this way lack sufficient versatility for the design of compact time-of-flight analyzers.

Analysis of existing solutions reveals that a universal mirror device capable of providing stable spatial and energetic ion focusing while maintaining a compact and simple analyzer design has not been found for multi-reflection TOFMSs. Known multi-stage designs do provide high performance, but they require complex matching elements and a large number of electrodes, making them unsuitable for compact devices.

3. The aim and objectives of the study

The objective of our study is to optimize a multi-reflection time-of-flight mass analyzer with transaxial mirrors by determining the operating modes of the transaxial mirrors that achieve spatial and energy time-of-flight focusing of the ion beam. This will enable high resolution and sensitivity in a compact analyzer design.

To achieve this goal, the following tasks were set:

– to define the geometric parameters of the mirrors and the electrode potentials that achieve spatial and energy time-of-flight focusing;

– to demonstrate the stability of volume ion beam trajectories in statistical Monte Carlo simulations for $N \geq 1000$ particles;

– to determine the mass resolution of the instrument based on the ion arrival time plot for a mass doublet with a difference of $\gamma = 0.0001$ and demonstrate that a resolution of 10,000 is achieved at the peak half-height.

4. The study materials and methods

4. 1. The object and hypothesis of the study

The object of our study is a multi-reflection time-of-flight mass spectrometer (TOFMS) based on transaxial electrostatic mirrors providing spatial and energy time-of-flight focusing of the ion beam. The hypothesis assumes that the transaxial mirrors generate an electrostatic field that provides simultaneous spatial and energy time-of-flight focusing of ions in the absence of additional focusing elements.

The following assumptions were adopted in our calculations:

– gaps between the electrodes are assumed to be infinitely narrow;

– the harmonic approximation is used for the potential describing the field of the mirrors;

– the influence of space charge is absent.

The following simplifications were accepted:

– a centered ion beam with a defined spatial and initial ion spread is considered;

– beams obtained in real pulsed ion sources are simulated.

4. 2. Electrostatic potential describing the transaxial mirror field

Any TOFMS contains at least three elements: a pulsed ion source, an ion receiver (detector), and a device (usually an ion mirror) between them to compensate for the energy spread that occurs in the pulsed source during ion packet formation. The use of gridless planar mirrors in TOFMSs allows for the design of devices with high-quality spatiotemporal focusing and zero temporal energy dispersion.

Such mirrors can be used, in particular, to design multi-pass time-of-flight mass spectrometers. Once the time-of-flight of one cascade is designated T_0, and the number of cascades N, the mass resolution of the mass spectrometer is then determined from the following expression

$$R_m = \frac{NT_0}{2\left(\Delta t_i + N\Delta t_0\right)} = \frac{T_0}{2\left(\frac{\Delta t_i}{N} + \Delta t_0\right)}. \quad (1)$$

Δt_i is the initial temporal width of the ion pulse, and Δt_0 is the time-of-flight aberration of a single cascade. According to formula (1), the resolution of a time-of-flight mass spectrometer can be increased by increasing the number of cascades N and decreasing the cascade aberrations Δt_0.

Thus, according to formula (1), it is sufficient to calculate one or two TOFMS cascades. Moreover, the number of cascades N should not be too large.

Difficulties arise in the corpuscular-optical calculation of electrostatic mirrors due to the fact that near the turning points of charged particles, the radii of curvature of their trajectories tend to zero. At the same time, the inclinations of the trajectories to the optical axis and the relative spread of particle energies increase indefinitely. These effects lead to deterioration of spatiotemporal focusing and limit the resolution of the device.

These difficulties can be overcome by integrating Newton's equations over the particle travel time rather than the trajectory equations. Numerical integration of Newton's equations is significantly simplified by the availability of analytical expressions for the potentials describing the electric fields of mirrors. Solutions to the Laplace equation in coordinates corresponding to the symmetry of the system are proposed in [12, 13]. These methods yield potentials that satisfy boundary conditions and are suitable for calculating the focusing properties of transaxial systems.

A three-electrode transaxial lens or mirror consists of two parallel plates cut by right circular cylinders of radius R_1 and R_1, whose axis coincides with the z-axis. Such a mirror is schematically depicted in Fig. 1. The figure also shows the accompanying Cartesian coordinate system x, y, z. The origin of the Cartesian coordinate system is located in the midplane of the mirror, which coincides with the xy-plane; V_0, V_1 and V_2 are the electrode potentials, and d is the distance between the plates. The gaps between the electrodes are assumed to be infinitely narrow. Far from the edges of the plates, the potential φ depends only on variables $\rho=\sqrt{x^2+y^2}$ and z in cylindrical coordinates ρ, ψ, z.

Introducing dimensionless variables [14]

$$\eta=\ln\frac{\rho}{R},\ \ \zeta=\frac{z}{R}, \tag{2}$$

where $R=\sqrt{R_1R_2}$, yields the following equation for the potential

$$e^{-2\eta}\frac{\partial^2\phi}{\partial\eta^2}+\frac{\partial^2\phi}{\partial\zeta^2}=0. \tag{3}$$

The harmonic component of the electrostatic potential $\varphi(\eta, \zeta)$ satisfies the two-dimensional Laplace equation and is a harmonic function of the dimensionless variables η and ζ. Therefore, the theory of functions of a complex variable (TFCV) can be used to calculate the potential. The analytical expression for the potential obtained in this way provides a good approximation of the potential $\varphi(\eta, \zeta)$ since it exactly satisfies the specified Dirichlet boundary conditions and, for $\rho \cong R$ ($\eta=0$), satisfies the two-dimensional Laplace equation. The variable ψ represents the angular coordinate characterizing the deviation of the particle trajectory from the axis. Since the electrode system has a significant extension along the angular direction, the dependence of the electrostatic potential on ψ can be neglected. This assumption is justified by the fact that the generated ion beam moves near the x-axis, and the transverse deviation of the particles is small.

In cylindrical coordinates, analytical expressions for the electrostatic potential of three-electrode transaxial mirrors can be written in the following form [15]

$$\phi(\rho,z)=V_2+(V_0-V_1)P_1\left(\frac{\rho}{R_1},z,R\right)+ \\ +(V_1-V_2)P_2\left(\frac{\rho}{R_2},z,R\right), \tag{4}$$

where

$$p_k\left(\tfrac{\rho}{R_k},z,R\right)=\frac{1}{\pi}\operatorname{arctg}\left(\frac{2\cos\frac{\pi}{d}z}{\left(\frac{\rho}{R_k}\right)^{\frac{\pi R}{d}}-\left(\frac{\rho}{R_k}\right)^{-\frac{\pi R}{d}}}\right),\ (k=1,2). \tag{5}$$

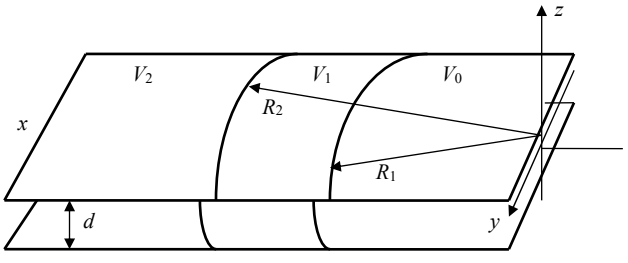

Fig. 1. Schematic representation of a transaxial mirror

This fairly simple analytical expression for the electrostatic potential of a three-electrode transaxial lens can also be used to calculate transaxial mirrors.

4. 3. Dimensionless Newton's equations

When studying the dynamics of a charged particle beam in multi-reflector transaxial systems, it is sufficient to consider the passage of charged particles through two mirrors, neglecting the pulse duration generated by the source, the duration of which can be reduced by increasing the number of cascades used. The equations of motion for a charged particle with charge q and mass $m=m_0(1+\gamma)$, where γ is the relative mass spread in the beam, in an electrostatic field with potential $\varphi(x, y, z)$ in dimensionless Cartesian coordinates x, y, z can be written as follows

$$\ddot{x}=F_k,\ \ \ddot{y}=F_y,\ \ \ddot{z}=F_z. \tag{6}$$

Here, the dimensionless potential $F(x,y,z)=\dfrac{\phi(x,y,z)}{V_0}$ is measured in V_0 units; the indices of F denote partial derivatives with respect to the corresponding Cartesian coordinates; the unit of length is taken to be d, the distance between the parallel planes of the transaxial mirror; the dots denote derivatives with respect to dimensionless time $\tau=t/\tau_0$, where

$$\tau_0=d\sqrt{\frac{m_0}{qV_0}}. \tag{7}$$

To calculate the derivatives of the potential included in equations (6), the following formulae for the derivatives of expressions (5) were used:

$$\frac{\partial P_k}{\partial\rho}=-\frac{\frac{2R}{R_kd}\cos\frac{\pi z}{d}\left[\left(\frac{\rho}{R_k}\right)^{\frac{\pi R}{d}-1}+\left(\frac{\rho}{R_k}\right)^{-\frac{\pi R}{d}-1}\right]}{\left[\left(\frac{\rho}{R_k}\right)^{\frac{\pi R}{d}}-\left(\frac{\rho}{R_k}\right)^{-\frac{\pi R}{d}}\right]^2+4\cos^2\frac{\pi}{d}z}. \tag{8}$$

$$\frac{\partial P_k}{\partial x}=\frac{\partial P_k}{\partial\rho}\frac{\partial P}{\partial x}=\frac{\partial P_k}{\partial\rho}\frac{x}{\rho},\ \ \frac{\partial P_k}{\partial y}=\frac{\partial P_k}{\partial\rho}\frac{\partial\rho}{\partial y}=\frac{\partial P_k}{\partial\rho}\frac{y}{\rho}. \tag{9}$$

$$\frac{\partial P_k}{\partial z}=\frac{\frac{2}{d}\sin\frac{\pi z}{d}\left[\left(\frac{\rho}{R_k}\right)^{\frac{\pi R}{d}}-\left(\frac{\rho}{R_k}\right)^{-\frac{\pi R}{d}}\right]^2}{\left[\left(\frac{\rho}{R_k}\right)^{\frac{\pi R}{d}}-\left(\frac{\rho}{R_k}\right)^{-\frac{\pi R}{d}}\right]+4\cos^2\frac{\pi z}{d}}. \quad (10)$$

The given values of derivatives (8) to (10) were substituted into the differentiated expression (4), thereby determining the right-hand sides of equations (6).

Fig. 2 shows a plot of the derivative of the dimensionless potential $F_z(x,0,0)=f_z(x)$ for a transaxial lens with $R_1=23d$, $R_2=25d$; $V_0=1$, $V_1=0.1$, $V_2=0.6$. Based on the resulting set of values, a table was generated, which was used to plot $f_z(x)$ as a function of the x coordinate in Visual Basic for Application (VBA) in Excel.

Fig. 2 shows the nature of the field strength variation in the midplane of the mirrors. It is evident that the field strength peaks at the indicated radii, where the potential differences are greatest. This field distribution determines the regions of effective ion focusing and allows one to evaluate the influence of electrode geometry on the spatiotemporal characteristics of the beam.

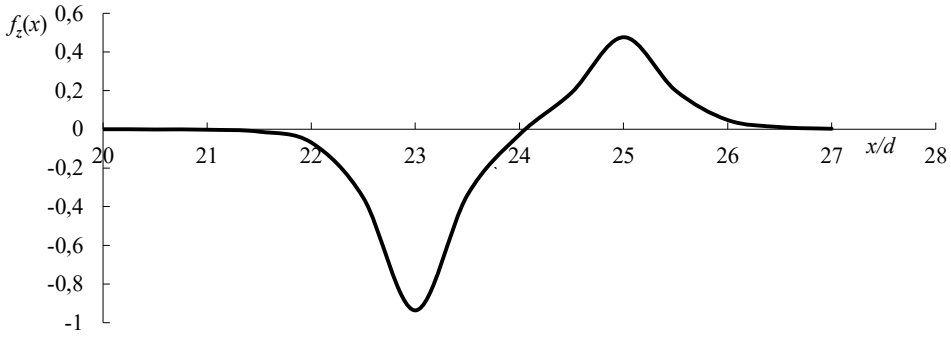

Fig. 2. Distribution of the derivative of the potential along the x-axis for a transaxial system in which $R_1=23d$, $R_2=25d$; $V_0=1$, $V_1=0.1$, $V_2=0.6$

5. Optimization results for a multi-reflection time-of-flight mass analyzer with transaxial mirrors

5. 1. Calculations of the geometry and electrostatic field of transaxial mirrors for spatial energy time-of-flight focusing

Newton's dimensionless equations (6) were integrated numerically using the Adams four-point method with automatic integration step selection. Acceleration points were found using the Krylov method of successive approaches. Numerical calculations were performed for transaxial mirrors with $R_1=23d$, $R_2=25d$; $V_0=1$, $0<V_1<1$, $V_2<0$. The unit length was chosen to be $d=1$ – distance between parallel planes of the transaxial mirror. The initial conditions simulated a circular centered ion source of radius $r_0=0.005$, the center of which is located in the out-of-field region in the midplane of the mirror at the point: $x_0=-14$, $y_0=1.85$, $z_0=0$. The axial trajectory was directed at an angle of $\alpha_0\cong 2.51°$ to the x-axis. When moving in the midplane of the mirror, where $z_0=\dot{z}_0=0$, the angle α_0 determines the inclination of the axial trajectory to the x-axis, which is the main optical axis of the mirror, and is determined from the following expression

$$\mathrm{tg}\alpha_0=\frac{\dot{y}_0}{\dot{x}_0}. \quad (11)$$

The initial conditions for the ion beam particles were specified as follows: $\dot{x}_0=\sqrt{2(1+\varepsilon)-\dot{y}_0^2-\dot{z}_0^2}$, where $\dot{y}_0=-0.062$, $|\dot{z}_0|\le 0.0002$, ε is the relative energy spread in the beam. The volume beam was modeled by changing the initial conditions as follows: $|\triangle\alpha|\le 0.0001$ rad, $|\varepsilon|\le 0.001$. With these initial condition changes, the paraxial approximation still holds fairly well. The relative integration accuracy was chosen to be $10^{-8}\div 10^{-9}$.

The results of the particle motion integration calculations are shown in Fig. 3–5. Fig. 3 demonstrates the behavior of the axial beam trajectory projected onto the midplane of the mirror, while Fig. 4, 5 depict the behavior of the beam trajectory projections in a vertical direction. In Fig. 3, the abscissa axis represents the values of the dimensionless variable x/d. Two variants of vertical beam focusing in the paraxial approximation were considered. The electrode potentials were selected to ensure spatial and energy time-of-flight focusing, and the detector D was positioned symmetrically to the position of the ion source S relative to the x-axis.

The first version of vertical focusing is shown in Fig. 4. This version was implemented with the following electrode potentials: $V_0=1$, $V_1=0.9725$, $V_2=-0.0937$.

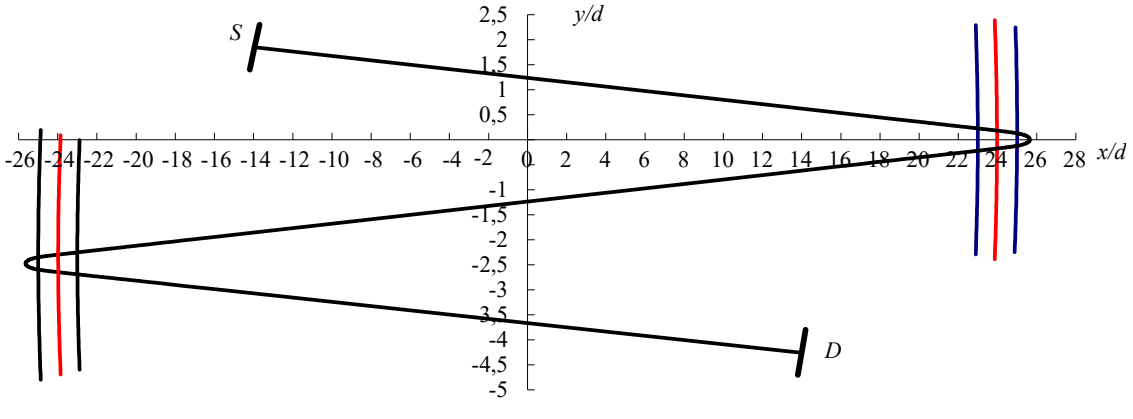

Fig. 3. Behavior of the axial beam trajectory in projection onto the midplane of the mirrors

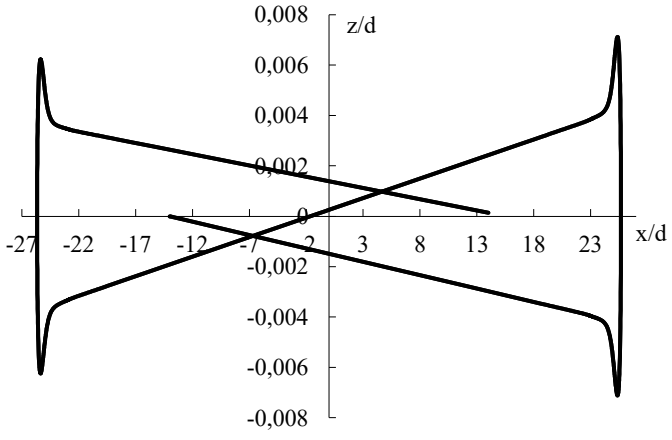

Fig. 4. Projections of particle trajectories emerging from the midplane onto the vertical direction

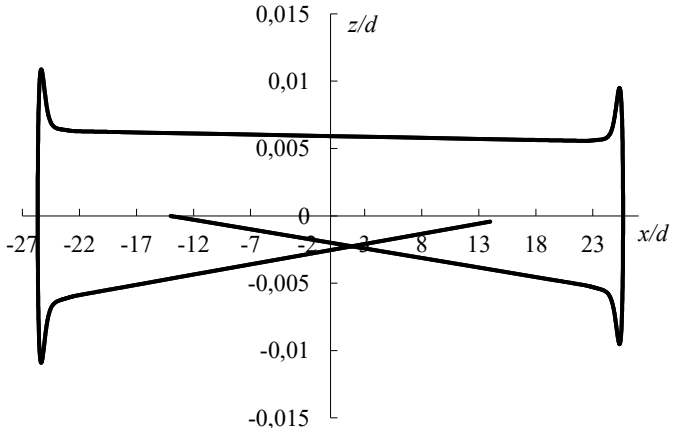

Fig. 5. Projections of particle trajectories emerging from the midplane onto the vertical direction

The particle flight time to the detector plane, which passes through the point $x_d = 14$ perpendicular to the axial beam trajectory, was also determined. For an axial trajectory ($\varepsilon = 0$), the arrival time at detector D is $\tau_{d0} = 98.57288$, while for particles moving along an axial trajectory with $\varepsilon = 0.001$, we obtain $\tau_{d1} = 98.57835$, and for $\varepsilon = -0.001$, we obtain an arrival time at the detector of $\tau_{d2} = 98.56828$.

The second variant of vertical focusing is shown in Fig. 5. It was implemented with the same electrode potentials: $V_0 = 1$ and $V_2 = -0.0937$, and a slightly modified potential $V_1 = 0.9641$. In this case, a parallel ion beam is formed in the gap between the mirrors. The time of flight of particles to the detector plane $x_d = 14$ was also determined. For an axial trajectory ($\varepsilon = 0$), the arrival time at detector D is $\tau_{d0} = 98.59036$, and for particles moving along an axial trajectory with $\varepsilon = 0.001$ we obtain $\tau_{d1} = 98.59579$, and for $\varepsilon = -0.001$ we obtain the arrival time at the detector $\tau_{d2} = 98.58581$. From these data it is evident that time-of-flight focusing by energy and simultaneous spatial focusing of the beam are carried out with sufficiently good accuracy.

5. 2. Modeling the behavior of a centered ion beam generated by a source in transaxial mirrors

The initial conditions for calculating the trajectories of charged particles in the ion beam during integration of equations (6) were modeled using the Monte Carlo method using the standard random number generator *Rnd*() and were specified as follows:

$$r_i = r_0 Rnd(),\ \psi_i = \rightleftarrows 2\pi Rnd(),$$

$$y_{i0} = r_i \cos\psi_i,\ z_{i0} = r_i \sin\psi_i,$$

$$x_{i0} = \rightleftarrows y_{i0} \tan\alpha_0,$$

$$\dot{x}_{i0} = \sqrt{2(1+\varepsilon_i) - \dot{y}_{i0}^2 - \dot{z}_{i0}^2},$$

$$\dot{y}_{i0} = r_i \sin\triangle\alpha_i,\ \dot{z}_{i0} = \sin\triangle\alpha_i. \quad (12)$$

Here, the indices $i, j = 1, 2, ..., N$ number the beam particles; the angle $\Delta\alpha_i$ determines the projection of the particle velocity vector onto the y- and z-axes. The quantities ε_i and $\Delta\alpha_i$ were specified by a normal distribution within $\pm 3\sigma$ and implemented using the Metropolis algorithm.

Fig. 6 shows the spatial configuration of a centered ion beam emerging from an ion source, projected onto coordinate planes for $N = 1000$.

For example, if we set $d = 1$ cm, the ion source diameter will be $2r_0 = 10^{-4}$ m, or 100 microns, which is quite consistent with the typical parameters of compact sources for laboratory mass spectrometers. These beam sizes ensure high ion density and stable trajectories in the initial acceleration region. The resulting spatial distributions serve as the basis for analyzing the focusing properties of the mirrors and allow us to move on to studying ion beam dynamics in a multi-reflection system.

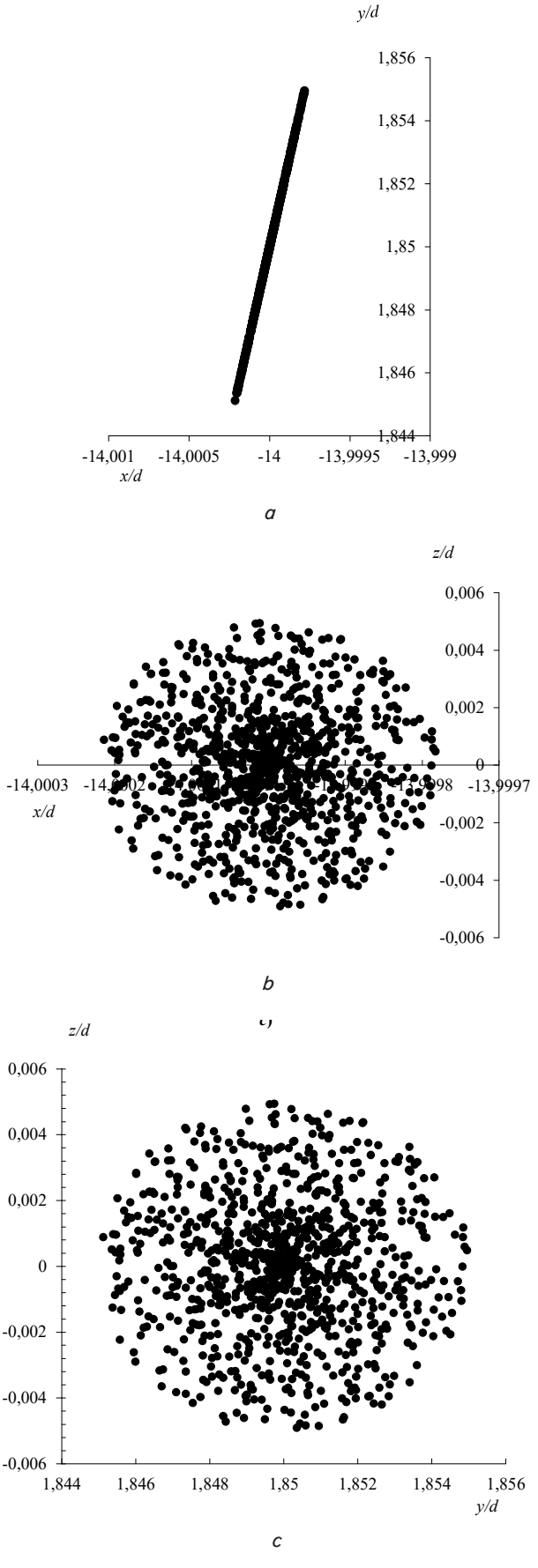

Fig. 6. Spatial configuration of a centered ion beam formed by a source: *a* — on the *yx*-plane; *b* — on the *zx*-plane; *c* — on the *zy*-plane

5. 3. Particle distribution in the detector plane and the resolving power of a time-of-flight mass analyzer

Dimensionless Newton equations (6) were integrated over dimensionless time τ for different initial conditions to the same final value τ_k. Some particles did not reach the detector plane, while others flew over it. In this case, the arrival time of charged particles at the detector was determined taking into account that near the detector plane, where the field is absent, particles move along rectilinear trajectories at a constant velocity. If, at time $\tau = \tau_k$ the particle was at point (x_k, y_k, z_k) and was moving with velocity $\left(\dot{x}_k, \dot{y}_k, \dot{z}_k\right)$, then the rectilinear portion of the projection of its trajectory onto the midplane is described by the following equation

$$y - y_k = k_k (x - x_k), \tag{13}$$

where

$$k_k = \mathrm{tg}\alpha_k = \frac{\dot{y}_k}{\dot{x}_k}. \tag{14}$$

It was assumed that the detector plane is located parallel to the *z*-axis and perpendicular to the axial trajectory, then its equation takes the form

$$y - y_{d0} = k_d (x - x_d), \tag{15}$$

where

$$k_d = -\frac{1}{\mathrm{tg}\alpha_{k0}} = \rightleftarrows -\frac{\dot{x}_{k0}}{\dot{y}_{k0}},$$

y_{d0} is the coordinate of the intersection of the axial trajectory with the detector plane. The coordinates of the intersection of projection (12) with the detector plane:

$$x_1 = \frac{k_k x_k - k_d x_k + y_{d0} - y_k}{k_k - k_d}.$$

$$y_1 = k_k \left(x_1 - x_k\right) + y_k x. \tag{16}$$

Now the time of arrival at the detector is determined from the following formula

$$\tau_d = \tau_{d0} \pm \frac{\sqrt{\left(x_1 - x_k\right)^2 + \left(y_1 - y_k\right)^2}}{\upsilon_{xy}}. \tag{17}$$

Here τ_{d0} is the time of arrival of the axial trajectory at the detector, the "+" sign is taken if the particle does not reach the plane of the detector, and the "–" sign is taken if it flies over the plane of the detector; and υ_{xy} is the projection of the velocity onto the *xy* plane.

$$\upsilon_{xy} = \sqrt{\dot{x}_k^2 + \dot{y}_k^2}. \tag{18}$$

Thus, the use of dimensionless Newtonian equations ensures high accuracy in calculating ion trajectories and flight times, allowing beam dynamics simulations to be performed without loss of versatility when changing mirror geometry and potentials.

The trajectories of charged particles in the ion beam were simulated; its passage through a system of two mirrors was considered. Fig. 7 shows the configuration of the ion beam

arriving at the detector plane. All $N = 1000$ particles emitted from the source, for a given beam configuration, reached the detector. The particle distribution in the detector plane is shown in Fig. 7, projected onto the xy and zy coordinate planes.

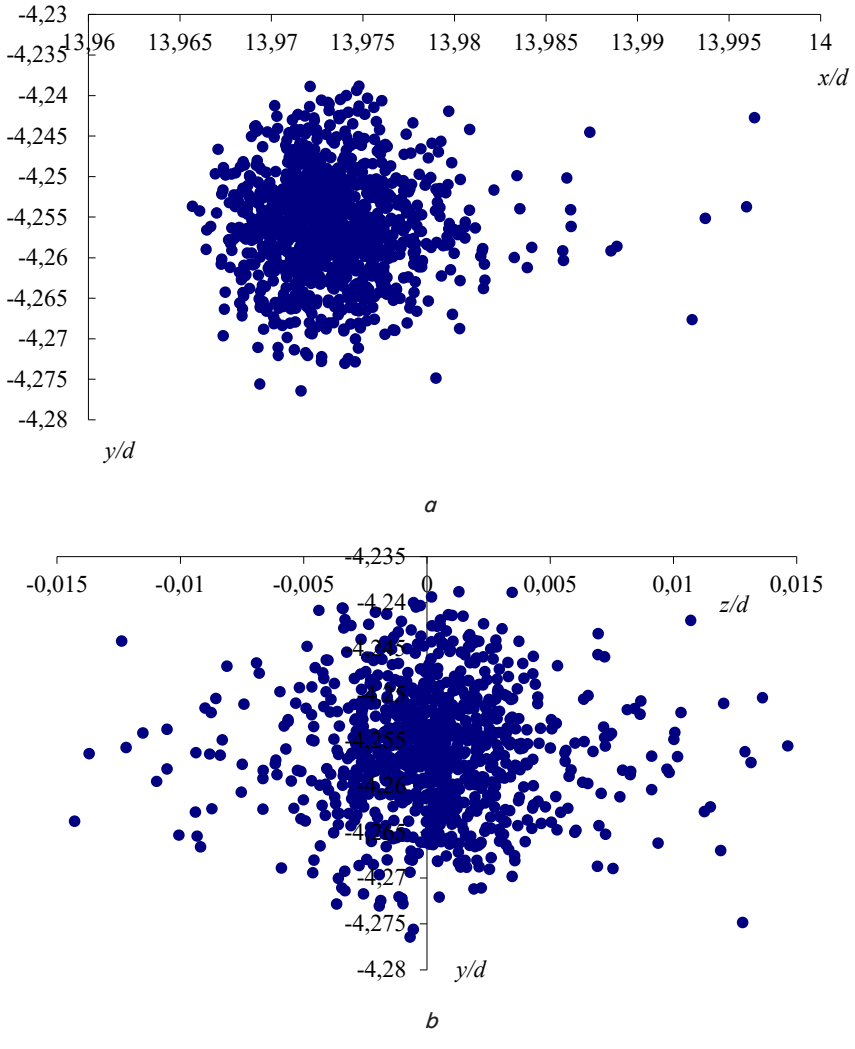

Fig. 7. Particle distribution in the detector plane: *a* — in the *xy* plane; *b* — in the *zy* plane

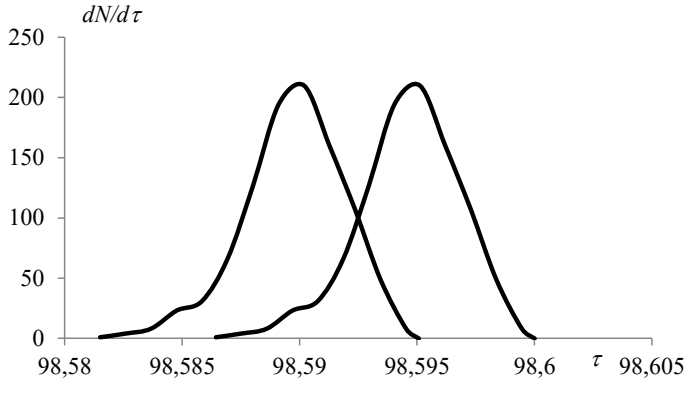

Fig. 8. Distribution of particles by their relative time of flight into the detector for a mass doublet with γ = 0 and γ = 0.0001

By using a diaphragm before the detector entrance and removing highly deflected particles (no more than 20 are collected), a distribution of particles by their relative times of flight into the detector is obtained, which is shown in the plot in Fig. 8 for a mass doublet with a relative mass difference of $\gamma = 0.0001$. Here, the dimensionless arrival time at the detector is plotted along the abscissa, and the number of particles is plotted along the ordinate. Thus, the resolution of the proposed mass analyzer is approximately 10,000 at half-maximum.

6. Modeling the time-of-flight mass spectrometer with transaxial mirrors: results and summary

Our calculation results shown in Fig. 3–5 demonstrate that the chosen mirror geometry $R_1 = 23d$, $R_2 = 25d$, as well as the electrode potentials, generate two modes of vertical spatial and energetic time-of-flight focusing of the ion beam. Under the first mode, a converging beam is formed in the detector at potential values $V_0 = 1$, $V_1 = 0.9725$, $V_2 = -0.0937$ (Fig. 4). Under the second mode, $V_0 = 1$, $V_1 = 0.9641$, $V_2 = -0.0937$, a nearly parallel beam is formed in the intermirror space. Fig. 5 shows that particle reflection occurs in the region of the negative potential, and the ion beam is focused toward the midplane. The difference in the transit times of particles with an energy spread $\varepsilon = \pm 0.001$ is no more than 0.01 dimensionless units; it is explained by the fact that particles with higher energy pass further into the region of negative potential where the particles are reflected, as a result of which their path becomes longer compared to ions with lower energy, thus all particles with higher and lower energy reach the detector simultaneously.

The axial trajectory for a two-mirror system, which also shows the location of the source and detector, located outside the field where the particle trajectories are straight, is shown in Fig. 3. The axial trajectory of the ion beam in the midplane was obtained using the appropriate methods of numerical integration of Newton's differential equations using the Adams method with automatic step selection, the acceleration points for which are found using the Krylov method of successive approaches. The programs used have been tested on a large number of solved problems [12–15].

Thus, the results of determining the geometric parameters of the mirrors and the electrode potentials confirm that the transaxial mirror provides spatial and energetic time-of-flight focusing, whereas known multi-reflection time-of-flight mass spectrometer designs with planar mirrors require the use of additional focusing electrodes [4–11].

Monte Carlo simulation of charged particle beam dynamics (12) at $N = 1000$ allowed us to obtain the instrumental characteristics of the proposed mass analyzer with transaxial mirrors. It was shown that a centered beam

with an initial radius of $r_0 = 0.005$ remains stable and virtually completely reaches the detector (Fig. 6). Translating the results to a physical scale ($d = 1$ cm) demonstrates that the beam diameter in the detector is approximately 100 μm, which meets the requirements for compact laboratory mass spectrometers. This stability is explained by the fact that the trajectories were calculated using exact dimensionless Newtonian equations, which make our results more universal for any real values of d and potentials V. This is also explained by the fact that two operating modes of the transaxial mirrors were selected, in which spatial and energy time-of-flight focusing are achieved. Unlike glider-based and hybrid systems [6, 9], which require additional trajectory correction, in the proposed system, centering is ensured by the mirror geometry itself and the analytical form of the potential. Thus, statistical Monte Carlo simulation confirmed the stability of the volume ion beam trajectories.

The mass resolution for the mass doublet with $\gamma = 0$ and $\gamma = 0.0001$ is $R_m \approx 10^4$ at half-maximum (Fig. 7, 8). This is a high value, exceeding the values obtained in most modern compact TOFMS systems [4–8], especially considering the absence of additional focusing elements. This value is achieved through simultaneous spatial and energetic time-of-flight focusing by the mirror itself, the presence of two stable modes, and the modeling of charged particle beam dynamics. Particle distribution plotted by their relative time-of-flight to the detector for the mass doublet was generated using Visual Basic for Application (VBA) in Excel. Thus, the results of determining the mass resolution of the instrument confirm that the proposed design provides high resolution at minimal structural complexity.

Limitations of this study include the fact that the gaps between the electrodes were assumed to be infinitely narrow, and we used a harmonic approximation for the potential describing the mirror field.

In subsequent studies, it is proposed to take into account the influence of space charge, take into account the width of the gaps in the mirrors, and model the fields of the mirrors using numerical methods: the finite element method and the integral equation method.

7. Conclusions

1. Our calculations of the geometry and electrostatic field of transaxial mirrors yielded parameters $R_1 = 23d$, $R_2 = 25d$, as well as potentials that achieve simultaneous spatial and energy time-of-flight focusing of ions. Two stable vertical focusing regimes were obtained, characterized by small variations in the potential V_1. This explains the stability of the centered ion beam's behavior and the fact that higher-energy ions travel deeper into the potential. Therefore, the trajectories of these particles become longer, and their flight times are longer, thereby arriving at the detector simultaneously with lower-energy particles. The difference in the flight times of particles with an energy spread of $\varepsilon = \pm 0.001$ is no more than 0.01 dimensionless units, confirming the implementation of energy focusing.

2. Monte Carlo simulation of the centered ion beam dynamics for $N = 1000$ particles with normal initial condition distributions showed that the generated source with a radius of $r_0 = 0.005$ maintains a centered beam structure in the detector plane, confirming trajectory stability and the absence of beam divergence. All ions reach the detector while maintaining compactness, and the beam diameter, when converted to the physical scale ($d = 1$ cm), is 100 μm. The proposed system differs from planar and hybrid TOFMSs in that it does not require additional focusing elements.

3. Simulation of the beam's flight to the detector plane in Visual Basic for Application (VBA) in Excel for a mass doublet with a relative difference of $\gamma = 0.0001$ showed that the mass resolution reaches $R \approx 10{,}000$ at the half-maximum of the peaks. This resolution is comparable to or superior to modern multi-reflector and hybrid systems but is achieved with a significantly simpler mirror design. Our results demonstrate the feasibility of using transaxial mirrors in compact, high-resolution TOFMSs.

Conflicts of interest

The authors declare that they have no conflicts of interest in relation to this study, including financial, personal, authorship, or other, which could affect the study and the results reported in this paper.

Financing

1. The work was carried out within the framework of a project with grant funding from the Ministry of Science and Higher Education of the Republic of Kazakhstan (AR22685992).

2. This work was carried out within the framework of a project with grant funding from the Ministry of Science and Higher Education of the Republic of Kazakhstan (AP23486969).

Data availability

The data will be provided upon reasonable request.

Use of artificial intelligence

The authors confirm that they did not use artificial intelligence technologies when creating the presented work.

Authors' contributions

Tilektes Zh. Shugayeva: Conceptualization, Methodology, Formal analysis, Software, Writing – original draft, Project administration; **Igor Spivak-Lavrov:** Methodology, Formal analysis, Validation, Supervision, Writing – review & editing; **Orda Baisanov:** Visualization, Data curation, Investigation; **Amangul Amantayeva:** Resources, Review, Discussion of results.

References

1. Wollnik, H. (2013). History of mass measurements in time-of-flight mass analyzers. International Journal of Mass Spectrometry, 349-350, 38–46. https://doi.org/10.1016/j.ijms.2013.04.023

2. Cotter, R. J. (1989). Time-of-flight mass spectrometry: An increasing role in the life sciences. Biological Mass Spectrometry, 18 (8), 513–532. https://doi.org/10.1002/bms.1200180803
3. Wollnik, H., Wada, M., Schury, P., Rosenbusch, M., Ito, Y., Miyatake, H. (2019). Time-of-flight mass spectrographs of high mass resolving power. International Journal of Modern Physics A, 34 (36), 1942001. https://doi.org/10.1142/s0217751x19420016
4. Meisel, Z., George, S. (2013). Time-of-flight mass spectrometry of very exotic systems. International Journal of Mass Spectrometry, 349-350, 145–150. https://doi.org/10.1016/j.ijms.2013.03.022
5. Knauer, S., Fischer, P., Marx, G., Müller, M., Rosenbusch, M., Schabinger, B. et al. (2019). A multi-reflection time-of-flight setup for the improvement and development of new methods and the study of atomic clusters. International Journal of Mass Spectrometry, 446, 116189. https://doi.org/10.1016/j.ijms.2019.116189
6. Yavor, M. I., Pomozov, T. V., Kirillov, S. N., Khasin, Y. I., Verenchikov, A. N. (2018). High performance gridless ion mirrors for multi-reflection time-of-flight and electrostatic trap mass analyzers. International Journal of Mass Spectrometry, 426, 1–11. https://doi.org/10.1016/j.ijms.2018.01.009
7. Rosenbusch, M., Wada, M., Chen, S., Takamine, A., Iimura, S., Hou, D. et al. (2023). The new MRTOF mass spectrograph following the ZeroDegree spectrometer at RIKEN's RIBF facility. Nuclear Instruments and Methods in Physics Research Section A: Accelerators, Spectrometers, Detectors and Associated Equipment, 1047, 167824. https://doi.org/10.1016/j.nima.2022.167824
8. Ayet San Andrés, S., Hornung, C., Ebert, J., Plaß, W. R., Dickel, T., Geissel, H. et al. (2019). High-resolution, accurate multiple-reflection time-of-flight mass spectrometry for short-lived, exotic nuclei of a few events in their ground and low-lying isomeric states. Physical Review C, 99 (6). https://doi.org/10.1103/physrevc.99.064313
9. Cooper-Shepherd, D. A., Wildgoose, J., Kozlov, B., Johnson, W. J., Tyldesley-Worster, R., Palmer, M. E. et al. (2023). Novel Hybrid Quadrupole-Multireflecting Time-of-Flight Mass Spectrometry System. Journal of the American Society for Mass Spectrometry, 34 (2), 264–272. https://doi.org/10.1021/jasms.2c00281
10. Dickel, T., San Andrés, S. A., Beck, S., Bergmann, J., Dilling, J., Greiner, F. et al. (2019). Recent upgrades of the multiple-reflection time-of-flight mass spectrometer at TITAN, TRIUMF. Hyperfine Interactions, 240 (1). https://doi.org/10.1007/s10751-019-1610-y
11. Jiang, J., Hua, L., Xie, Y., Cao, Y., Wen, Y., Chen, P., Li, H. (2021). High Mass Resolution Multireflection Time-of-Flight Secondary Ion Mass Spectrometer. Journal of the American Society for Mass Spectrometry, 32 (5), 1196–1204. https://doi.org/10.1021/jasms.1c00016
12. Spivak-Lavrov, I. (2016). Analytical Methods for the Calculation and Simulation of New Schemes of Static and Time-of-Flight Mass Spectrometers. Advances in Imaging and Electron Physics, 45–128. https://doi.org/10.1016/bs.aiep.2015.10.001
13. Spivak-Lavrov, I. F., Kalimatov, T. S., Shugaeva, T. Z. (2019). Prismatic mass analyzer with the conical achromatic prism and transaxial lenses. International Journal of Mass Spectrometry, 444, 116180. https://doi.org/10.1016/j.ijms.2019.116180
14. Spivak-Lavrov, I. F., Nurmukhanova, A. A., Shugaeva, T. Zh. (2019). Mass analyzer with a conic achromatic prism and transaxial lenses. Scientific Instrumentation, Saint Petersburg, 29 (1), 116–125.
15. Spivak-Lavrov, I. F., Shugaeva, T. Zh., Sharipov, S. U. (2020). Solutions of the Laplace equation in cylindrical coordinates, driven to 2D harmonic potentials. Advances in Imaging and Electron Physics, 181–193. https://doi.org/10.1016/bs.aiep.2020.06.006